A Boundary Condition for Guderley's Converging Shock Problem

J.J. Ruby,[1, a)] J.R. Rygg,[1, b)] J.A. Gaffney,[2] B. Bachmann,[2] and G.W. Collins[1, b)]
[1)]*Department of Physics and Astronomy, and Laboratory for Laser Energetics, University of Rochester, Rochester, New York, 14627, USA*
[2)]*Lawrence Livermore National Laboratory, Livermore, California 94550, USA*

(Dated: 26 November 2019)

The Guderley model of a self-similar imploding shock based on the group invariance of the flow equations is a powerful tool in understanding the behavior of converging shock waves. Two modifications described here improve the predictions of observable quantities in spherical-shock wave experiments. First, a non-infinite boundary condition is established by the isentropic release of the outer pressure. Second, a two-temperature system of ions and electrons allows description of higher temperatures while conserving energy and without perturbing the overall hydrodynamics of the solution. These modifications of the Guderley model improve the prediction of the observables in laser driven spherical shock experiments in reference to a one dimensional (1-D) hydrodynamics code.

I. INTRODUCTION

Converging shock waves appear in diverse locations throughout nature such as in inertial confinement fusion experiments,[1–3] supernovae explosions,[4,5] and cavity collapses.[6] Guderley[7] found a self-similar solution that can be used to describe all these systems across the different size and temporal scales found in nature. Despite significant work[8–10] exploring the numerical properties of the Guderley solution and using it to benchmark hydrodynamic codes,[11–13] little work exists in using the solution to understand experimental results. Work has been done to treat the boundary of self-similar solutions, such as the Guderley, in order to better relate them to numerical hydrodynamic codes[12–14]. This work describes a new boundary condition and scheme for the treatment of temperature, motivated by experimental comparison.

Shock wave experiments in spherical geometry are challenging to perform and diagnose and thus direct isolated measurements of the extreme physical states or processes accessed with such convergent experiments are usually beyond state of the art techniques, so design and analysis of such convergent experiments often employ radiation hydrodynamic codes.[2] Semi-analytic solutions to hydrodynamic systems offer a valuable baseline for comparison to integrated models.[12] These solutions are used to inform experimental observations in diverse regimes of spherical shocks, for example such as in rarefied gas.[15] A direct analogue to these solutions is challenging to create experimentally[16], so modifications of the solution are sometimes necessary[16,17] to understand experiments outside the realm of the solution such as ones containing magnetic fields[18,19]. The scheme presented in this work when combined with previous work,[15,20–22] makes for a powerful tool in quantitatively determining the states and processes implicit to convergent experiments, and is an important step toward constraining physical models from a collection of experimental observables.

[a)]Electronic mail: jruby@lle.rochester.edu.
[b)]Also at Mechanical Engineering Department, University of Rochester, Rochester, New York, 14627, USA

A. Review of the Guderley Problem

The Guderley problem of a converging shock wave has been described extensively elsewhere.[1,8,23] The solution starts with the non-viscous ideal conservation equations of fluid mechanics:

$$\begin{aligned} \frac{\partial \vec{u}}{\partial t} + \vec{u}\cdot\vec{\nabla}\vec{u} + \frac{\vec{\nabla}P}{\rho} &= 0, \\ \frac{\partial \rho}{\partial t} + \vec{\nabla}\cdot(\rho\vec{u}) &= 0, \\ \frac{\partial S}{\partial t} + \vec{u}\cdot\vec{\nabla}S &= 0, \end{aligned} \tag{1}$$

where $\vec{u}$ is the velocity field, P, ρ, and S are the gas pressure, density, and entropy, respectively, and the three equations correspond to the conservation of momentum, mass, and energy (entropy), respectively. Additionally, for this solution an ideal adiabatic equation of state is assumed, taking the form

$$\begin{aligned} PV &= Nk_{\mathrm{B}}T, \\ S &= \ln\left(P\rho^{-\gamma}\right), \end{aligned} \tag{2}$$

where V is the volume, N is the number of particles, k_{B} is the Boltzmann constant, and γ is the ratio of specific heats or the adiabatic index. Finally, invoking spherical or cylindrical symmetry the problem is reduced to a 1-D radial set of equations of the form

$$\begin{aligned} \frac{\partial u}{\partial t} + u\frac{\partial u}{\partial r} + \frac{1}{\rho}\frac{\partial P}{\partial r} &= 0, \\ \frac{\partial \rho}{\partial t} + \frac{1}{r^{n-1}}\frac{\partial}{\partial r}\left(r^{n-1}\rho u\right) &= 0, \\ \frac{\partial S}{\partial t} + u\frac{\partial S}{\partial r} &= 0, \end{aligned} \tag{3}$$

where n is a parameter that sets the geometry of the problem taking on the values 1, 2, and 3 for planar, cylidrical, and spherical geometries, respectively. These equations evolve in a self-similar fashion with the similarity co-ordinate ξ defined as

$$\xi = \xi_0 \frac{r/r_0}{|t/t_0|^{\alpha}}. \tag{4}$$

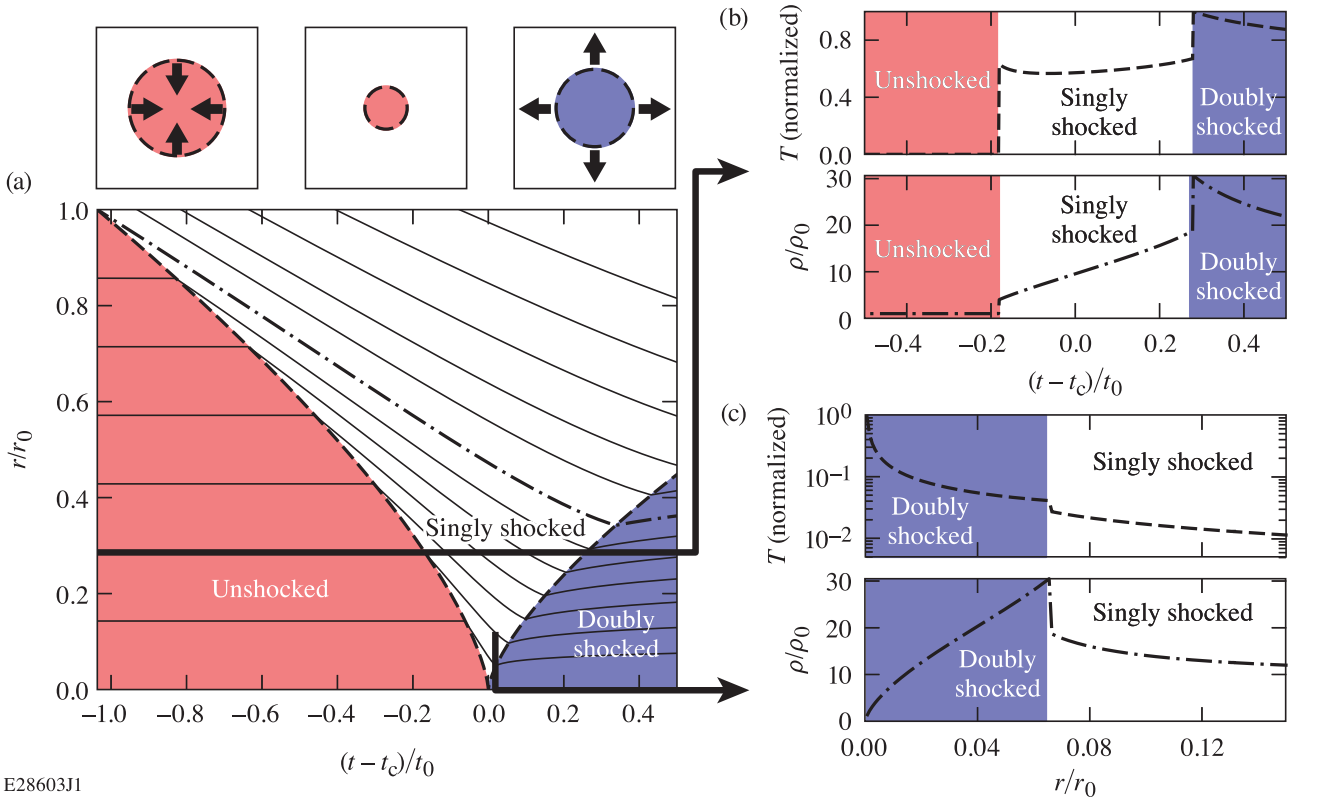

FIG. 1. The particle trajectories (solid black curves), r_0 particle trajectory (dashed-dotted black curve), and shock trajectory (dashed black curve) in the Guderley solution for a particular set of parameters ($\kappa = 0$, $\gamma = 5/3$, $\alpha \approx 0.6883768$, and $n = 3$). Note that in the Guderley solution the trajectories starting from r_0 are not significant because the flow extends out to infinity and is self-similar. The shading represents different regions of flow: unshocked (red), singly shocked (white), and doubly shocked (blue). Top left is a cartoon of the physical system: a spherical (or cylindrical) shock (dashed) is converging inward into unshocked material (red) as seen in the first and second frames. The shock then rebounds and moves back outward through the singly shocked (white) material leaving doubly shocked material (blue) in its wake. Note that the white region extends out to infinity. Marked with thick black lines are the locations of a temporal and a radial lineout of the temperature and density profiles shown to the right. The temporal profile is shown in (b) and the radial profile is shown in (c).

The choice of this coordinate is derived from the scaling symmetries that exist in the equations.[1] ξ introduces the parameters ξ_0, r_0, t_0, and α. Both ξ_0 and α help to define the shock trajectory and strength, and there is a unique α for the choice of γ, the ratio of specific heats or the adiabatic index, and geometric factor, n. It is important to note that α is independent of boundary conditions, but ξ_0 depends on the specifics of the boundary, in particular the strength of the pressure wave at infinity. Scaling parameters r_0 and t_0 set the spatial and temporal scales of the system being modeled. This allows the fluid properties to be given in terms of the similarity coordinate. In order to solve the system, only three of the fluid properties (particle velocity, sounds speed, density, temperature, pressure, entropy, etc.) need to be defined and the rest can be derived. Different references choose to define different properties. As an example[10,24], the flow velocity, density, and sound speed are given as

$$\begin{aligned} u(r,t) &= \frac{\alpha r}{t} U(\xi), \\ \rho(r,t) &= \rho_0 \left(\frac{r}{r_0}\right)^{\kappa} G(\xi), \\ c(r,t) &= \frac{\alpha r}{t} C(\xi), \end{aligned} \tag{5}$$

where there are an additional two parameters: ρ_0 is a reference density and κ is the density exponent defining the initial density profile. Inserting the scaled quantities into the flow equations allows one to derive a set of autonomous ordinary differential equations of the form

$$\frac{dU}{dC} = f(U,C). \tag{6}$$

These equations can be solved numerically and then transformed back to the radius and time space[1,13,24]. The parameters introduced in this solution are given in Table I.

TABLE I. Parameters in the Guderley solution to the converging shock-wave problem. Note that one of r_0, t_0, and ξ_0 can be defined in terms of the other two so they are not all independent.

r_0	Radial scaling factor
t_0	Temporal scaling factor
ξ_0	Shock strength parameter
γ	Adiabatic index
n	Geometric factor
κ	Density profile parameter
ρ_0	Density scaling factor

B. The Guderley Solution

The particle and shock trajectories that result from solving the Guderley problem provide insight into the dynamics of a converging shock wave. These trajectories are shown in Fig. 1 where the temporal axis is shifted by t_c, the time that the shock reaches the center, $r = 0$. The slope of the profiles is determined by the equation of state, namely the γ used, but the general features of the solution are independent of γ. The particle trajectory originating from $r/r_0 = 1$ is the dashed-dotted line. This trajectory has no unique significance in the Guderley solution because the flow extends out to infinity and is self-similar, but in experimental configurations there is usually a reference radius that carries significance such as an outer boundary of material. This boundary will be discussed in Sec. II

The density and temperature profiles are critical when describing shock waves in nature. The right-side top and bottom of Fig. 1 show temporal and spatial lineouts of the temperature and density, respectively, denoted by the arrows in the particle trajectory plot. The temperature at fixed radius is relatively steady in time between the two shock events. Conversely, the temperature is extremely steep in its radial profile with the temperature peak at $r = 0$ for all times after the shock collapse. The density is shocked as expected according to the strong shock condition to $\rho/\rho_0 = (\gamma+1)/(\gamma-1)$. After that point, the density continues to rise, a consequence of the material converging into a smaller volume. Finally, after re-shock the material relaxes and the density falls off. A single fluid temperature is shown but a scheme for separate treatment of electron and ion temperatures will be addressed in Sec. III.

II. FINITE BOUNDARY CONDITIONS

The self-similarity of the Guderley solution means the flow extends out to infinity. This implies that the shock wave is supported for all time and that the problem describes a system of infinite mass. In real physical systems, the finite boundary conditions often plays a key role in the dynamics, necessitating a treatment of the boundary condition. The simplest condition that can be used is to track the flow from a reference point, for example r_0, which may correspond to the outer boundary of an experimental target (dashed-dotted line in Fig. 1), and truncate the solution outside of that boundary. This scheme is valid while the pressure at the boundary is held constant, supporting the wave dynamics for the duration of the shock. The support of the pressure wave in the Guderley solution is a problem when the pressure is not held at the outer boundary indefinitely, such as in laser-driven shock experiments.

When the pressure at the boundary is released, a decompression wave is launched, changing the fluid property profiles. To model this, a released density profile of the form

$$\rho(r) = \rho_R \left(\frac{R_{\text{out}} - r}{R_{\text{out}} - R_{\text{in}}} \right)^{\varepsilon} \tag{7}$$

is assumed, based previous solutions to isentropic release waves in imploding media using the conservation of mass.[25] In this work, ε will be left as a free parameter that will be system specific. Here R_{in} and R_{out} are the inner edge and outer edge of the release wave, respectively, and ρ_R is the value of the density at the inner edge of the release wave, given by the density of the original Guderley solution. R_{out} is the boundary of the system beyond which there is no material. R_{in} is calculated using the sound speed in the compressed and moving material. Since the sound speed and density are given by the Guderley solution, the only unknown in the density profile is R_{out}. To find R_{out}, conservation of mass is used. The mass contained in the shell of material bounded by R_{in} and R_{c}, the location of the outermost fluid element, must equal the mass within the new released profile:

$$M = \int_{R_{\text{in}}}^{R_{\text{c}}} \rho_{\text{G}}(r, t_{\text{i}}) 4\pi r^2 \text{d}r = \int_{R_{\text{in}}}^{R_{\text{out}}} \rho_R \left(\frac{R_{\text{out}} - r}{R_{\text{out}} - R_{\text{in}}} \right)^{\varepsilon} 4\pi r^2 \text{d}r \tag{8}$$

where $\rho_{\text{G}}(r, t_{\text{i}})$ is the undisturbed radial Guderley density profile at time t_{i}. Solving the integral on the right hand side results in a third order polynomial for R_{out} given as

$$\begin{aligned} aR_{\text{out}}^3 + bR_{\text{out}}^2 + cR_{\text{out}} + d &= 0 \\ a &= \frac{1}{3+\varepsilon} - \frac{2}{2+\varepsilon} + \frac{1}{1+\varepsilon} \\ b &= \left(\frac{4}{2+\varepsilon} - \frac{3}{3+\varepsilon} - \frac{1}{1+\varepsilon} \right) R_{\text{in}} \\ c &= \left(\frac{3}{3+\varepsilon} - \frac{2}{2+\varepsilon} \right) R_{\text{in}}^2 \\ d &= -\left(\frac{R_{\text{in}}^3}{3+\varepsilon} + \frac{M}{4\pi\rho_R} \right). \end{aligned} \tag{9}$$

Solving this polynomial at each time step gives the trajectory of the outer edge of the release wave. This process is truncated when the inner edge of the release begins to interact with the rebounding shock wave. When this occurs, the trajectory of the outer edge is then extrapolated and the density at the inner edge of the release is solved by rearranging the polynomial to get

$$\rho_{\text{R}} = \frac{M}{4\pi} \left(aR_{\text{out}}^3 + bR_{\text{out}}^2 + cR_{\text{out}} - \frac{R_{\text{in}}^3}{3+\varepsilon} \right)^{-1}. \tag{10}$$

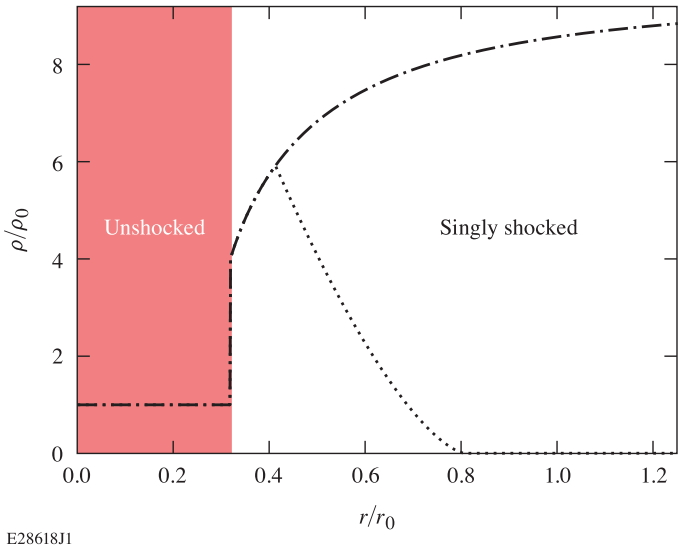

FIG. 2. A comparison of the Guderley solution radial density profiles before the time of shock collapse for the same parameters used in Fig. 1 and a release wave launched at $t = 0.45\ t_0$ and $\varepsilon = 3/2$. The original Guderley result (dashed-dotted black curve) is shocked up to a compression ratio of 4 (corresponding to the strong shock condition for $\gamma = 5/3$) and then rises to a peak value of just below 10 as a result of the converging material behind the wave. The profile that includes the release wave (dotted black curve) also is shocked to the same compression ratio of 4 and rises beyond that because of converging material but the release wave can be seen around $r/r_0 = 0.45$. The density in the released region falls according to Eq. (7) reaching zero at the outer extent of the release region. The released density profile has a peak compression ratio about 35% smaller than that of the standard solution. The shaded regions correspond to the shading shown in Fig. 1.

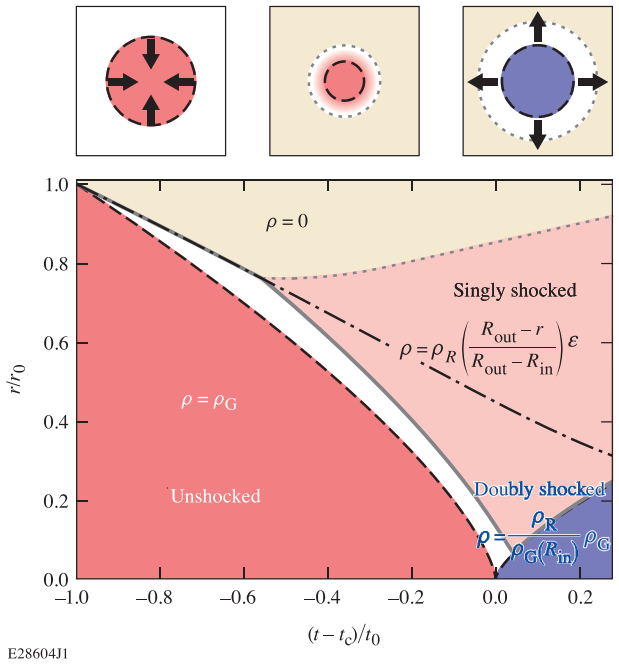

FIG. 3. Different wave trajectories in the Guderley solution with the release wave model. The shock front (dashed black curve), r_0 particle boundary (dashed-dotted black curve), and shading of the regions all correspond to Fig.1. The inner edge of the release wave (solid gray curve) and outer edge of the release wave (dotted gray curve) are also shown. Different regions are labeled with the density within that region: Outside of the release, there is no material (beige shading); interior to the release, the density is given from the Guderley solution (red and white shading); within the release, density is given by the functional form assumed (light-red shading); and within the doubly shocked region, the density is scaled according the released density value (blue shading). The top shows a cartoon of the physical system (similar to Fig. 1). In the cartoon note now that the shock (dashed curve) and outer edge of the release wave (dotted curve) are shown. The shading corresponds to the lower part of the figure where the beige denotes $\rho = 0$ and the white and light-red regions denote the released density profile. Now there is no material outside of the release wave, so the boundary no longer extends to infinity.

The density profiles for the standard Guderley solution and the release modification are compared in Fig. 2.

As the shock moves out re-shocking material, it will eventually interact with the released material, modifying the density, pressure, and temperature. This is treated by scaling the density behind the second shock by the ratio of the released density value and the Guderley density value at the location of the re-shock:

$$\rho_{\text{reshock}} = \frac{\rho_R}{\rho_G(+R_{in})}\rho_G, \tag{11}$$

where $+R_{in}$ is referencing the density value on the singly shocked side of the discontinuity (the white region in Figs. 1 and 3). This is done in order to preserve the shock condition which is determined by the equation of state, through γ. The different trajectories and density regions are shown in Fig. 3.

Finally, following from the adiabatic relationship $PV^\gamma =$ constant and the ideal equation of state, the temperature and pressure profiles in the released material are given by

$$\begin{aligned} P &= P_0\left(\frac{R_{out}-r}{R_{out}-R_{in}}\right)^{\varepsilon\gamma}, \\ T &= T_0\left(\frac{R_{out}-r}{R_{out}-R_{in}}\right)^{\gamma}. \end{aligned} \tag{12}$$

The modified temperature profile can now be used as the single fluid temperature inherent in the Guderley solution. A two-fluid temperature calculation is discussed in Sec. III.

III. TWO-FLUID TEMPERATURE TREATMENT

The Guderley problem is usually solved in terms of entropy (as developed in Sec. I A) or sound speed [as given in Eqs. (5)] both of which can be related to the temperature of the fluid. Working in the framework already established for the problem, the entropy or sound speed can easily be converted into the temperature through the equation of state, for example, $c = \sqrt{\gamma k_B T/m}$, where m is the mass of the particles being considered.

One primary result from the Guderley solution is that the temperature, while being a single-fluid temperature, reaches

extremely high values at the collapse point because of the strong shocks in the system. The combination of high temperatures and short time scales that are associated with shock waves necessitates the treatment of ions and electrons as two fluids with separate temperatures. The presence of these large temperature gradients can be addressed through other methodologies, for example by including heat conduction.[26] This work includes a two fluid treatment, specifically with the goal of reproducing experimental observables that have separate dependencies on the electron and ion temperatures as shown in Sec. IV.

The separation of the temperature into two different populations begins with how the energy is partitioned into those populations. Throughout this work, charge neutrality is assumed such that $n_e = \bar{Z} n_i$, the number density of electrons in a fluid element is equal to the average ionization state times the number density of ions. In shocked material the particles will move with the same velocity so the energy imparted to the particle is proportional to the mass of the particle. In other words the ratio of the energy goes as the ratio of the masses

$$\frac{E_i}{E_e} = \frac{\bar{A} m_u}{m_e} \approx 1823\,\bar{A}, \tag{13}$$

where m_e is the electron mass and $\bar{A} m_u$ is the ion mass, with $\bar{A}$, the average atomic mass number and m_u, the atomic mass unit. The temperature is proportional to the energy for an ideal gas population of particles given by $E = N k_B T/(\gamma - 1)$ (assuming that γ is the same for electrons and ions), so the temperature of the population is also proportional to the mass of the particles comprising the population. The shock leaves the electrons and ions with a temperature ratio of

$$\frac{T_i}{T_e} = \frac{\bar{A} m_u}{\bar{Z} m_e} \approx 1823 \frac{\bar{A}}{\bar{Z}}, \tag{14}$$

following from the energy of each population, determined by their masses. Here $\bar{Z}$ is the average ionization state of the ions, which determines how many electrons there are per ion.

The strong shock wave in the problem leaves the electrons and ions far out of equilibrium. Considering τ_{ei} as the characteristic time scale of equilibration between electrons and ions, the electron-electron and ion-ion time scales, τ_{ee} and τ_{ii}, are much smaller, i.e., they equilibrate faster as a result of the greater efficiency of the energy transfer between collisions of particles with the same mass.[27] Since this is the case, the electron and ion distributions are assumed to be Maxwellian at all times but relax to different temperatures, T_e and T_i.

The equilibration is treated in a way that leaves the single-fluid temperature of the Guderley solution, T_G, unperturbed, in order not to change the hydrodynamic evolution of the system. The electron and ion temperatures are constrained to obey

$$\frac{1}{\gamma_i - 1} n_i T_i + \frac{1}{\gamma_e - 1} n_e T_e = \frac{1}{\gamma - 1} n T_G, \tag{15}$$

i.e., the energy in any given fluid element remains the same and is just partitioned between the electrons and ions. Assuming that $\gamma_i = \gamma_e$, $n_e = \bar{Z} n_i$, and $n = n_i + n_e$ the relationship between the temperatures is given by

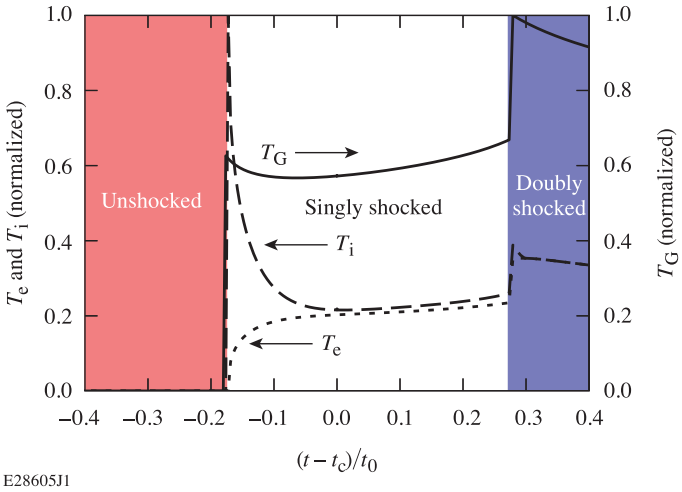

FIG. 4. A comparison of the Guderley solution radial temperature profile [solid black curve; as seen in Fig. 1 (b)] with the electron (dotted black curve) and ion (dashed black) radial temperature profiles for the same parameters used in Fig. 1 and τ_{ei} given by Spitzer. The ion temperature increases much more drastically than the electron temperature from the first shock due to the large difference in mass between the particles as discussed in the text. The two populations then begin to equilibrate and almost come to equilibrium before the second shock. The second shock boosts the ions a bit higher again, and the two species equilibrate shortly thereafter.

$$T_i + \bar{Z} T_e = (1 + \bar{Z}) T_G, \tag{16}$$

Using this constraint, the electrons and ions are equilibrated according to[27]

$$\frac{dT_e}{dt} = \frac{T_i - T_e}{\tau_{ei}}. \tag{17}$$

Here τ_{ei} is usually given as a function of electron temperature as well. The Guderley solution gives $T_G(r,t)$ so using this and the constraint on the energy partitioning gives an ODE for the electron temperature as a function of time for a given radius r_i:

$$\frac{dT_e}{dt} = (1 + \bar{Z}) \left(\frac{T_G(r_i, t) - T_e}{\tau_{ei}(T_e)} \right). \tag{18}$$

This can then be numerically solved, and the ion temperature as a function of time is given as $T_i = (1 + \bar{Z}) T_G(r_i, t) - \bar{Z} T_e(t)$. The temperature dependence of $\bar{Z}$ can also be entered into this equation, but for this work the calculation of $\bar{Z}$ was made using the initial ion temperature post-shock before equilibration. Fig. 4 shows a comparison of the temporal profiles of the Guderley, electron, and ion temperatures.

IV. EXPERIMENTAL USAGE

The temperature equilibration and release modification of the Guderley solution are used to predict the observables of

TABLE II. Parameters in the Guderley solution to the converging shock wave with the addition of the release model and temperature equilibration. The values selected for Sec. IV are given.

r_0	Radial scaling factor	443 μm
ξ_0	Shock-strength parameter	151.6 μm/ns$^\alpha$
t_0	Temporal scaling factor	$(r_0/\xi_0)^{1/\alpha} = 4.58$ ns
γ	Adiabatic index	1.5
α	Derived from γ	0.7044
n	Geometric factor	3
κ	Density profile parameter	0
ρ_0	Density scaling factor	1.04 g/cm^3
ε	Release density exponent	7/2
t_r	Time release is launched	0.45 t_0
τ_{ei}	Electron-ion equipartition time	Eq. (21)

a high-energy-density experiment. The predictions are compared to the 1-D hydrodynamics code *Lilac*.[28] The experimental configuration includes a strong laser-driven spherical shock in a solid deuterated polystyrene ball that is 0.890 mm in outer diameter. This is a type of experiment conducted on the *Omega* Laser system[29] at the Laboratory for Laser Energetics. The key observables of interest are x-rays and deuterium-deuterium fusion neutrons produced around the time of shock collapse. To properly model these in the modified Guderley solution, the addition of an ionization model and x-ray opacity model is necessary; neutron scattering is neglected here due to its negligible effect on calculating the total neutron yield. Neutron scattering is important for higher order moments of the neutron spectrum which are not calculated in the current framework but can be added in future studies. The ionization model from Hu et al.[30] is used, providing a Saha-like framework for calculating the ionization levels in CH (the isotopic difference between CH and CD is neglected). Tabulated opacity values[31] are used and the emission is assumed to be emitted radially. The choice of ionization model and opacity values are used in order to make comparison to *Lilac*, with the same models being used in both. A benefit of this methodology is that different models can be easily implemented and the sensitivity to these models can be explored. The x-ray emission is calculated assuming only Bremsstrahlung emission,[1,23,32] due to the lack of spectral lines in the region of experimental observation in the few keV x-ray energy range, according to

$$J_\nu = \frac{\sqrt{2^{11}\pi^3}}{3}\frac{(\frac{e^2}{4\pi\varepsilon_0})^3\bar{Z}^2 n_e^2}{m_e^2 c^3 \bar{Z}\sqrt{3kT_e/m_e}} e^{-\frac{h\nu}{kT_e}} \quad \left[Js^{-1}m^{-3}Hz^{-1}\right] \tag{19}$$

and the neutron emission is calculated according to

$$\frac{d^2N}{dtdV} = \frac{1}{2}n_D^2 < \sigma v >_{DDn} \left[\frac{\text{neutrons}}{m^3 s}\right] \tag{20}$$

where $< \sigma v >_{DDn}$ is the deuterium-deuterium thermal reactivity as given by, for example, Bosch and Hale[33]. All quantities are in S.I. units and the resulting units are given in brackets.

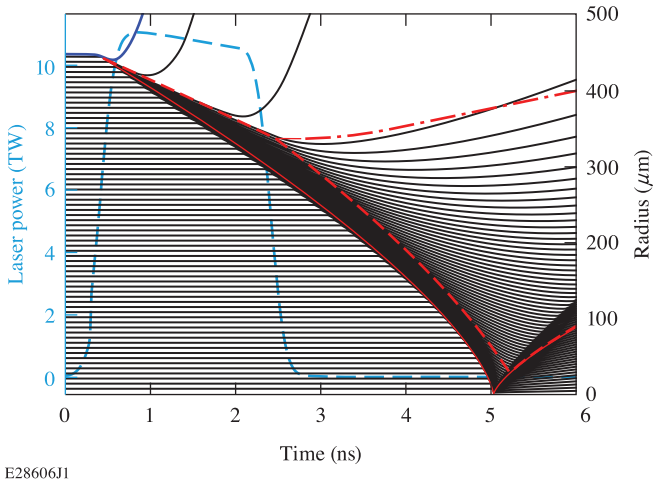

E28606J1

FIG. 5. Trajectory comparison for the *Lilac* particles (black) and the modified Guderley solution shock (solid red curve), inner release (dashed red curve), and outer release (dashed-dotted red curve) trajectories. Shock and release trajectories are seen to be in agreement,with the ingoing trajectory never deviating more than 5% between the two. The release behavior similarly agree until around the time of shock collapse where the release accelerates in the *Lilac* code. The laser pulse used in the *Lilac* simulation (light-blue dashed curve; left axis) is shown. The start of both the shock wave and the release wave in the modified Guderley model was chosen based on the beginning and end of the laser pulse, respectively.

A. Prediction of observables

The parameters of the Guderley solution including the modifications are chosen based on the experimental setup or comparison to the hydrodynamics code. The parameters are given in Table II. Many of the values used are given by nominal target specifications (n, ρ_0, r_0, κ) or laser configurations (t_r, t_0); ε is chosen based on previous literature on shock releases[25] and τ_{ei} is given by Spitzer[27] as

$$\tau_{ei} = \frac{3m_e\bar{A}m_u k_B^{3/2}}{8\sqrt{2\pi}n_i\bar{Z}^2\ln(\Lambda)(e^2/4\pi\varepsilon_0)}\left(\frac{T_e}{m_e}+\frac{T_i}{\bar{A}m_u}\right) \quad [s], \tag{21}$$

where all quantities are in S.I. units, the resulting units are given in brackets and $\ln(\Lambda)$ is the Coloumb Logarithm given[27] as

$$\Lambda = \frac{3(k_B T_i)^3}{2\sqrt{\pi n_e}\bar{Z}(e^2/4\pi\varepsilon_0)^{3/2}}. \tag{22}$$

The choice of γ and ξ_0 follows from matching the initial strength (pressure) of the shock and the time of shock collapse between the *Lilac* and the Guderley solution. Once the full solution is established, a set of common experimental observables is calculated in order to compare. These quantities include the total neutron yield, given as the integral of Eq. (20) over volume and time; the total x-ray yield, given as the integral of Eq. (19) over volume, time, and spectral frequency; and the x-ray energy where the peak of the spectrum is located. The x-ray quantities are dependent on the absorption,

TABLE III. Comparison of the deuterium-deuterium fusion neutron yields (Y_N), x-ray (Y_X) and peak x-ray spectral energy from the different model configurations. The comparison includes the 1-D Lagrangian hydrodynamic code *Lilac* and the Guderley (Gud) solution with equal electron and ion temperatures ($T_e = T_i$), with the temperature equilibration (τ_{ei}), with equal electron and ion temperatures and the release modification ($T_e = T_i$ + Rel), and with the temperature equilibration and the release modification (τ_{ei}+Rel).

Simulation	Y_N	Y_X (mJ)	Spectral Peak (keV)
Lilac	7.320×10^6	1.151	7.1
Gud ($T_e = T_i$)	6.625×10^6	0.078	10.0
Gud (τ_{ei})	7.742×10^6	0.016	15.0
Gud ($T_e = T_i$ + Rel)	5.874×10^6	1.410	7.0
Gud (τ_{ei} + Rel)	7.116×10^6	0.895	8.0

which is a strong function of the density, while the neutron emission is primarily a function of temperature. The release modification, which primarily changes the density profile, has the most leverage on the x-ray emission quantities, while the temperature equilibration scheme determines the temperature affecting both x-ray and neutron emission.

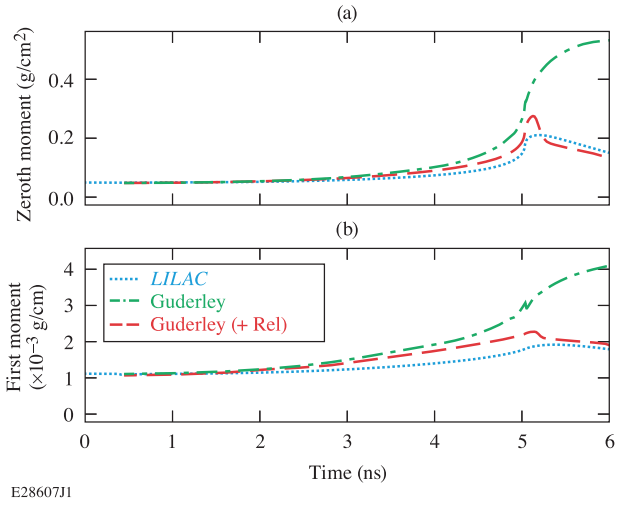

FIG. 6. Comparison of the (a) zeroth and (b) first radial moments of the density distributions as a function of time for *Lilac* (blue dotted curve), the Guderley solution with the equilibration model but no release model (τ_{ei} ; green dashed-dotted curve), and the Guderley solution with the equilibration and release models (τ_{ei} + Rel ; red dashed curve) as described in Table III. Note that the Guderley solutions with $T_e = T_i$ and with the temperature equilibration have the same moments of the density distribution so only one is shown.

B. Comparison to *Lilac*

The comparison simulation was run in *Lilac* using nonlocal heat transport,[34] the same opacity[31] and ionization[30] values used in the Guderley calculations, and the *sesame* equation-of-state tables.[35] As was previously stated, the only tuning required for the modified Guderley model to match the *Lilac* results was based on the initial (ablation) pressure and the time of shock collapse. The *Lilac* simulation has an ablation plasma resulting from the direct laser illumination on the outside of the target, which can contribute to self-emission quantities; *Lilac* quantities were calculated using only the region inside of the ablation plasma, i.e. only contributions from the shock-generated states. The resulting trajectories are compared in Fig. 5. The trajectories show good agreement, deviating less than 5% on the ingoing trajectories, with the largest deviations occurring with the release around the time of shock collapse and with the shock post-collapse. The inner release trajectory is calculated according to the sound speed so the difference in trajectory is due to a difference in local sound-speed between *Lilac* and the Guderley model. Since the sound speed is dictated by the equation of state deviations of the used equation of state from an ideal gas account for the differences. The post-collapse shock trajectory is unmodified by the release in this model, which accounts for the Guderley shock diverging more slowly than the *Lilac* shock post-collapse. This is not, however, a critical period of these experiments because by this time most observable quantities have already been produced. The neutron and x-ray emission quantities are compared in Table III. The quantities are calculated for the *Lilac* simulation and the Guderley solution with and without the release model both for the fully equilibrated case and the case with dynamic equilibration. The neutron yield is primarily a function of the ion temperature, which is notably under-predicted in both $T_e = T_i$ cases. The x-ray quantities are functions of electron temperature, but they primarily depend on the mass density due to the attenuation of the x-rays. The models without the boundary treatment under-predict the x-ray yield and over-predict the peak spectral energy because only the high-energy x-rays are able to escape the system. The model with the equilibration and boundary treatment addresses both of these issues and is within 3%, 30%, and 13% for the neutron yield, x-ray yield, and spectral peak, respectively.

The x-ray emission is dominated by the absorption that is determined by the opacity and areal density (ρR) of the material. Fig. 6 compares the zeroth and first radial moments of the density distribution as a function of time. The zeroth moment gives the average areal density, $\langle \rho R \rangle$, the ratio of the first and zeroth moments gives an average radius, and the second moment is directly proportional to the mass. The first three moments are given by

$$\begin{aligned} \text{0th Moment} &= \int_0^\infty \rho(r)\mathrm{d}r, \\ \text{1st Moment} &= \int_0^\infty r\rho(r)\mathrm{d}r, \\ \text{2nd Moment} &= \int_0^\infty r^2\rho(r)\mathrm{d}r. \end{aligned} \tag{23}$$

Since mass is conserved throughout all of the models, the second moments are trivially identical throughout, so the comparison is limited to the zeroth and first moments.

Figure 6 shows that the standard Guderley model greatly over-predicts both of the moments. The zeroth moment of the modified-Guderley solution is larger than *Lilac* by about

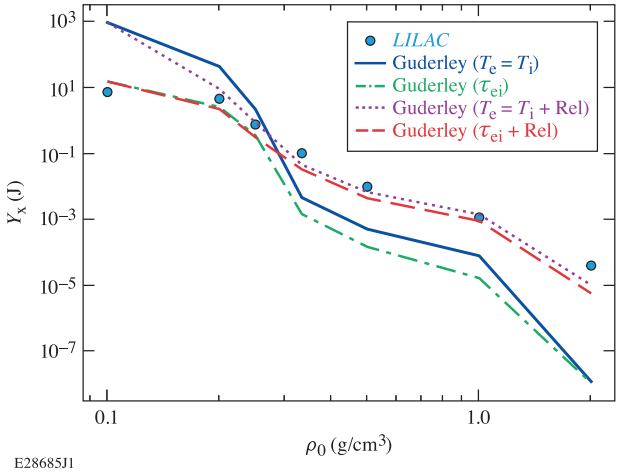

FIG. 7. Comparison of different models' predictions of x-ray yield as a function of initial density of the targets scaled from the nominal density ($\rho_0 = 1.04\ g/cm^3$). In the limit of lower density, the temperature equilibration is the more important modification, because the electron and ion fluids are far out of equilibrium due to the presence of higher temperatures and lower densities. As the density increases, the equilibration becomes less important (because the electrons and ions are much closer to equilibrium) and the release wave modification becomes more important. This agreement between the full model (τ_{ei} + Rel) and *Lilac* is best over the entire density space sampled. The full model has the same trend as the hydrocode but is displaced by some amount that can be attributed to the difference in equilibration models used in *Lilac* versus the Guderley model. All *Lilac* simulations were run with the same conditions as shown earlier and only the initial density of the target was varied. Each Guderley fit was done as described in the text, namely by matching the time of shock collapse and the initial pressure of the shock.

20% around the time of shock collapse. This is caused by the different timing of the release wave late in time, which is seen in Fig. 5. The difference in the zeroth moment around the time of peak x-ray emission (≈ 5 ns) corresponds to a greater areal density and is the reason for the lower x-ray yield (Table III) and harder emission predicted by the Guderley solution with release resulting from greater absorption. The first moment is also larger in the Guderley solution with release by about 20% before the time of shock collapse, but after collapse, the value is much closer to *Lilac* below about 5%.

Figure 7 shows how the x-ray yield scales as a function of the initial density for the different model shown in Table III. At lower densities, the attenuation is minimized and the electrons and ions are far out of equilibrium, so the solutions with and without the dynamic equilibration converge to the same values, respectively. At higher densities, the electrons and ions fully equilibrate very quickly but the attenuation is magnified, so the solutions with and without the release model converge to the same values. Only the fully modified Guderley model is able to reproduce the scaling of the x-ray yield over the entire density space considered.

V. CONCLUSIONS

The Guderley solution of an imploding shock wave with the addition of a boundary condition and electron-ion energy partitioning is effective at reproducing the simulated behavior of a high-energy-density experiment of interest. The particle trajectories of the Guderley solution with the release model boundary condition and *Lilac* simulations are consistent. Self-emission quantities compared between the Guderley solution and the *Lilac* simulation are within about 10% or less for most quantities when the complete Guderley system with boundary condition is considered. The favorable comparison between the hydrodynamics code and the Guderley solution with temperature equilibration and the release model demonstrates that the physics contained in the Guderley model is sufficient to explain most of the system. Additionally, similarity in the experimental quantities predicted by the two models demonstrates that these measurements are not sensitive to the additional physics contained in the hydrodynamics code, such as thermal conduction and radiation transport.

This model and similar models of this type are a critical step toward understanding which physics dominates a particular experimental setup and the physical mechanisms that can be probed using current observations. Additionally, this model has fewer parameters than a typical hydrodynamics code and can be better constrained by a limited set of experimental data when doing a model-fitting through, for example, a Bayesian framework, presenting a path forward in understanding which aspects of fundamental physics are dominant in integrated high-energy-density experiments.

ACKNOWLEDGMENTS

This material is based upon work supported by the Department of Energy National Nuclear Security Administration under Award Number DE-NA0003856, the U.S. Department of Energy, Office of Science, Office of Acquisition and Assistance under Award No. DE-SC001926, the University of Rochester, and the New York State Energy Research and Development Authority.

This report was prepared as an account of work sponsored by an agency of the U.S. Government. Neither the U.S. Government nor any agency thereof, nor any of their employees, makes any warranty, express or implied, or assumes any legal liability or responsibility for the accuracy, completeness, or usefulness of any information, apparatus, product, or process disclosed, or represents that its use would not infringe privately owned rights. Reference herein to any specific commercial product, process, or service by trade name, trademark, manufacturer, or otherwise does not necessarily constitute or imply its endorsement, recommendation, or favoring by the U.S. Government or any agency thereof. The views and opinions of authors expressed herein do not necessarily state or reflect those of the U.S. Government or any agency thereof.

[1] S. Atzeni and J. M. ter vehn, *The Physics of Inertial Fusion Beam Plasma Interaction, Hydrodynamics, Hot Dense Matter*, 1st ed. (Oxford University Press, Oxford, 2004).

[2]T. R. Boehly, V. N. Goncharov, W. Seka, S. X. Hu, J. A. Marozas, D. D. Meyerhofer, P. M. Celliers, D. G. Hicks, M. A. Barrios, D. Fratanduono, and G. W. Collins, "Multiple spherically converging shock waves in liquid deuterium," Phys. Plasmas **092706** (2011), 10.1063/1.3640805.

[3]J. Lindl, "Development of the indirect drive approach to inertial confinement fusion and the target physics basis for ignition and gain," Phys. Plasmas **3933** (1995), 10.1063/1.871025.

[4]M. Fink, W. Hillebrandt, and F. K. Ropke, "Double-detonation subchandrasekhar supernovae: synthetic observables for minimum helium shell mass models," Astrophys. J. **719** (2010), 10.1088/0004-637X/719/2/1067.

[5]M. Kromer, S. A. Sim, M. Fink, F. K. Ropke, I. R. Seitenzahl, and W. Hillebrandt, "Double-detonation supernovae of sub-chandrasekhar mass white dwarfs," Astron. Astrophys. **476** (2007), 10.1051/0004-6361:20078438.

[6]C. Ohl, T. Kurz, R. Geisler, O. Lindau, and W. Lauterborn, "Bubble dynamics, shock waves and sonoluminescence," Philos. Trans. Royal Soc. A **357** (1999), 10.1098/rsta.1999.0327.

[7]G. Guderley, "Starke kugelige und zylindrische verdichtungsstobe in der nahe des kugelmittelpunktes bzw. der zylinderachse," Luftfahrtforschung **19** (1942).

[8]S. Ramsey, J. Kamm, and J. Bolstad, "The guderley problem revisited," Int. J. of Comput. Fluid D **26**, 79–99 (2012).

[9]P. Hafner, "Strong convergent shock waves near the center of convergence: a power series solution," SIAM J. Appl. Math **48** (1988), 10.1137/0148076.

[10]R. F. Chisnell, "An analytic description of converging shock waves," J. Fluid Mech. **354**, 357–375 (1998).

[11]S. Doebling and N. Woods, "Exactpack: An open-source software package for code verification," `https://github.com/lanl/ExactPack/blob/master/README.md` (18 August 2017).

[12]S. Ramsey, P. Ivancic, and J. Lilieholm, "Verification assessment of piston boundary conditions for lagrangian simulation of compressible flow similarity solutions," Journal of Verification, Validation, and Uncertainty Quantification **0211003** (2016).

[13]S. Ramsey and J. Lilieholm, "Verification assessment of piston boundary conditions for lagrangian simulation of the guderley problem," Journal of Verification, Validation, and Uncertainty Quantification **031001** (2017).

[14]H. Hornung, D. Pullin, and N. Ponchaut, "Verification assessment of piston boundary conditions for lagrangian simulation of compressible flow similarity solutions," Acta Mechanica (2008).

[15]M. Liverts and N. Apazidis, "Limiting temperatures of spherical shock wave implosion," Phys. Rev. Lett. **116** (2016), 10.1103/PhysRevLett.116.014501.

[16]S. Ramsey and R. Baty, "Piston driven converging shock waves in a stiffened gas," Phys. Fluids **31** (2019).

[17]S. Ramsey, E. Schmidt, Z. Boyd, J. Lilieholm, and R. Baty, "Converging shock flows for a mie-gruneisen equation of state," Phys. Fluids **30** (2018).

[18]D. Pullin, W. Mostert, V. Wheatley, and R. Samtaney, "Converging cylindrical shocks in ideal magnetohydrodynamics," Phys. Fluids **26** (2014).

[19]A. Chauhan, R. Arora, and A. Tomar, "Convergence of strong shock waves in non-ideal magnetogasdynamics," Phys. Fluids **30** (2018).

[20]J. Rygg, "Shock convergence and mix dynamics in inertial confinement fusion," Ph.D. Thesis, MIT (2006).

[21]H. J. Haubold and R. W. John, "Analytical representation of the thermonuclear reaction rate and fusion energy production in a spherical plasma shock wave," Plasma Phys. **23** (1981), 10.1088/0032-1028/23/5/002.

[22]E. B. Goldman, "Numerical modeling of laser produced plasmas: the dynamics and neutron production in dense spherically symmetric plasmas," Plasma Phys. **15** (1973), 10.1088/0032-1028/15/4/005.

[23]Y. Zeldovich and Y. Raizer, *Physics of Shock Waves and High-Temperature Hydrodynamic Phenomena* (Dover Publications, Mineola, NY, 2002) vol. I, Chap. 12, Sec. 2, p. 794.

[24]R. Lazarus, "Self-similar solutions for converging shocks and collapsing cavities," SIAM J. Appl. Math **18** (1981).

[25]M. Basko and J. M. ter Vehn, "Asymptotic scaling laws for imploding thin fluid shells," Phys. Rev. Lett. **88** (2002), 10.1103/PhysRevLett.88.244502.

[26]P. Reinicke and J. M. ter Vehn, "The point explosion with heat conduction," Phys. Fluids. A: Fluid Dynamics **3** (1991).

[27]L. Spitzer and Jr., *Physics of fully ionized gases* (Interscience Publishers, New York, 1956).

[28]J. Delettrez, R. Epstein, M. C. Richardson, P. A. Jaanimagi, and B. L. Henke, "Effect of laser illumination nonuniformity on the analysis of time-resolved x-ray measurements in uv spherical transport experiments," Phys. Rev. A **36** (1987), 10.1103/PhysRevA.36.3926.

[29]T. Boehly, D. Brown, R. Craxton, R. Keck, J. Knauer, J. Kelly, T. Kessler, S. Kumpan, S. Loucks, S. Letzring, F. Marshall, R. McCrory, S. Morse, W. Seka, J. Soures, and C. Verdon, "Initial performance results of the omega laser system," Opt. Commun. **133** (1997), 10.1016/S0030-4018(96)00325-2.

[30]S. Hu, L. Collins, V. Goncharov, J. Kress, R. McCrory, and S. Skupsky, "First-principles investigations on ionization and thermal conductivity of polystyrene for inertial confinement fusion applications," Phys. Plasmas **23** (2016), 10.1063/1.4945753.

[31]S. Hu, L. Collins, J. Colgan, V. Goncharov, and D. Kilcrease, "Optical properties of highly compressed polystyrene: An ab initio study," Phys. Rev. B **96** (2017), 10.1103/PhysRevB.96.144203.

[32]J. Colvin and J. Larsen, *Extreme Physics: Properties and Behavior of Matter at Extreme Conditions* (Cambridge University Press, 2014).

[33]H.-S. Bosch and G. Hale, "Improved formulas for fusion cross-sections and thermal reactivities," Nucl. Fusion **32** (1992), 10.1088/0029-5515/32/4/I07.

[34]V. N. Goncharov, O. V. Gotchev, E. Vianello, T. R. Boehly, J. P. Knauer, P. W. McKenty, P. B. Radha, S. P.Regan, T. C. Sangster, S. Skupsky, V. A. Smalyuk, R. Betti, R. L. McCrory, D. D. Meyerhofer, and C. Cherfils-Cerouin, "Early stage of implosion in inertialconfinement fusion: Shock timing andperturbation evolution," Phys. Plasmas **13** (2006), 10.1063/1.2162803.

[35]B. I. Bennett, J. D. Johnson, G. I. Kerley, and G. T. Rood, "Recent developments in the sesame equation-of-state library," Los Alamos National Laboratory, Los Alamos, NM, Report LA-7130 (1978), 10.2172/5150206.